SUPPLEMENTARY INFORMATION

Supplementary figures

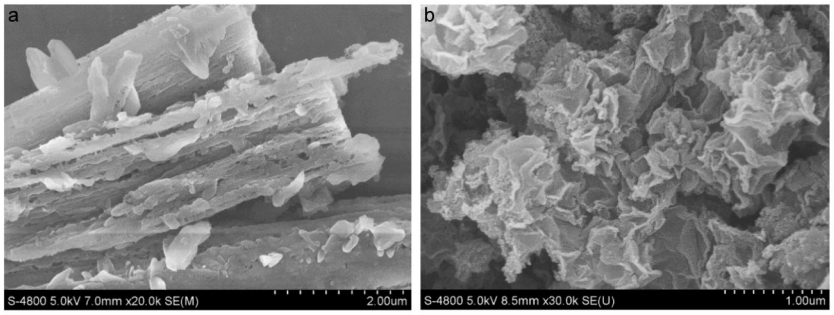

Supplementary Fig. 1 | a, SEM images of NC. **b,** SEM images of Fe_{SAC}-NC.

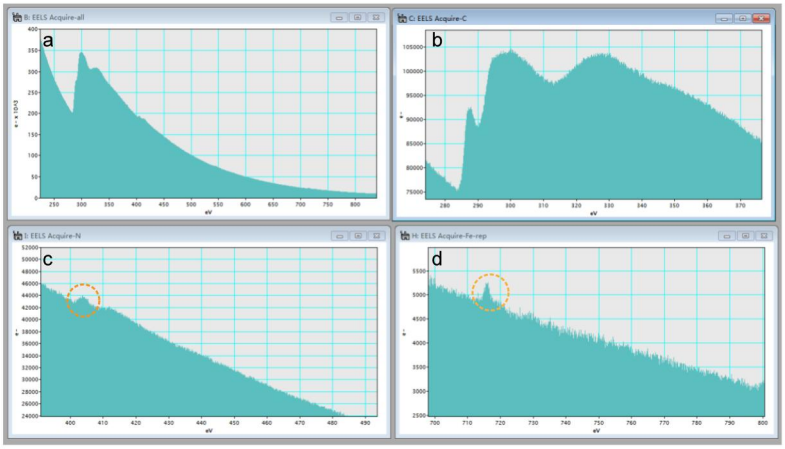

Supplementary Fig. 2 | EELS point spectrum of Fe_{SAC}-NC. **a,** full spectrum. **b,** C spectrum. **c,** N spectrum. **d,** Fe spectrum.

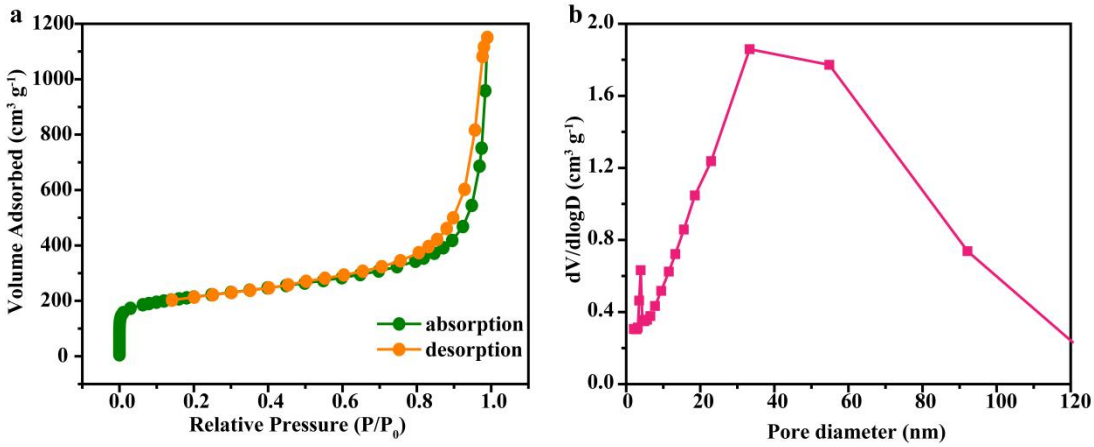

Supplementary Fig. 3 | a, N_2 adsorption-desorption curves of Fe_{SAC}-NC. **b,** Pore distribution curve of Fe_{SAC}-NC.

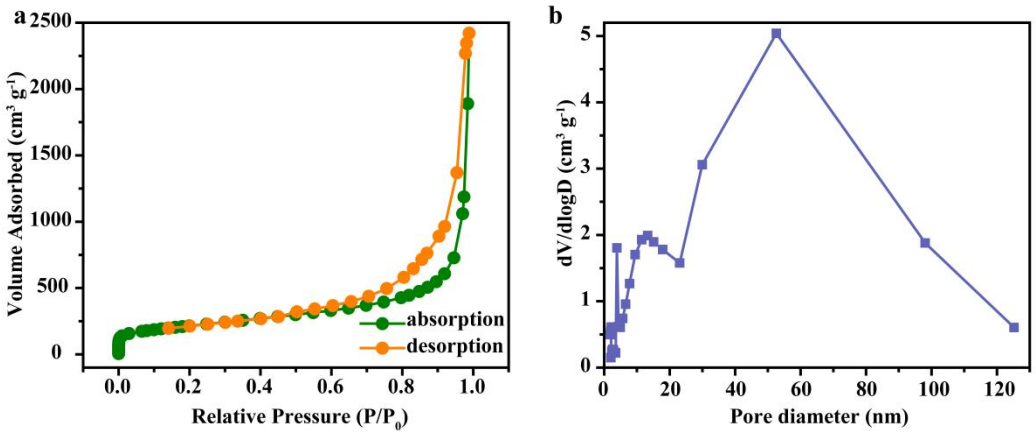

Supplementary Fig. 4 | a, N_2 adsorption-desorption curves of FeN_4. **b,** Pore distribution curve of FeN_4.

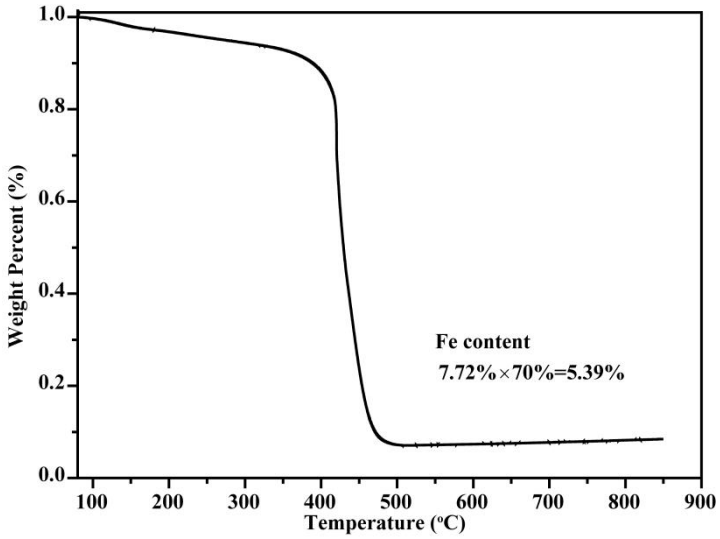

Supplementary Fig. 5 | TGA curve of Fe_{SAC}-NC tested in air ambient.

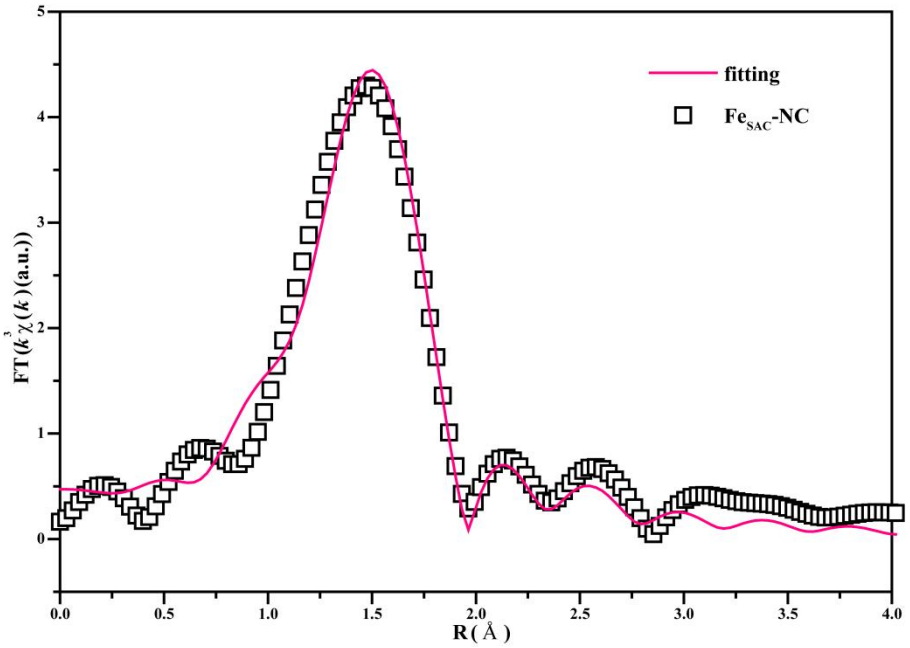

Supplementary Fig. 6 | k^3-weighted Fourier transform spectra of Fe_{SAC}-NC and corresponding fitting curve.

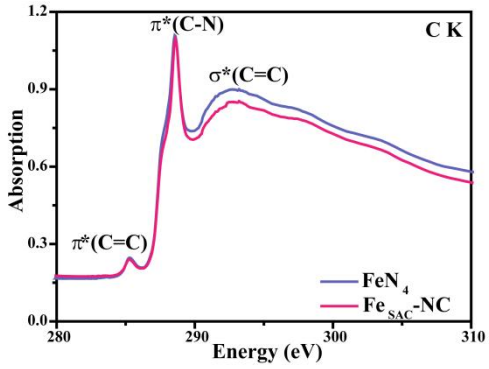

Supplementary Fig. 7 | The normalized XANES spectra at the C K-edge of FeN_4 and Fe_{SAC}-NC.

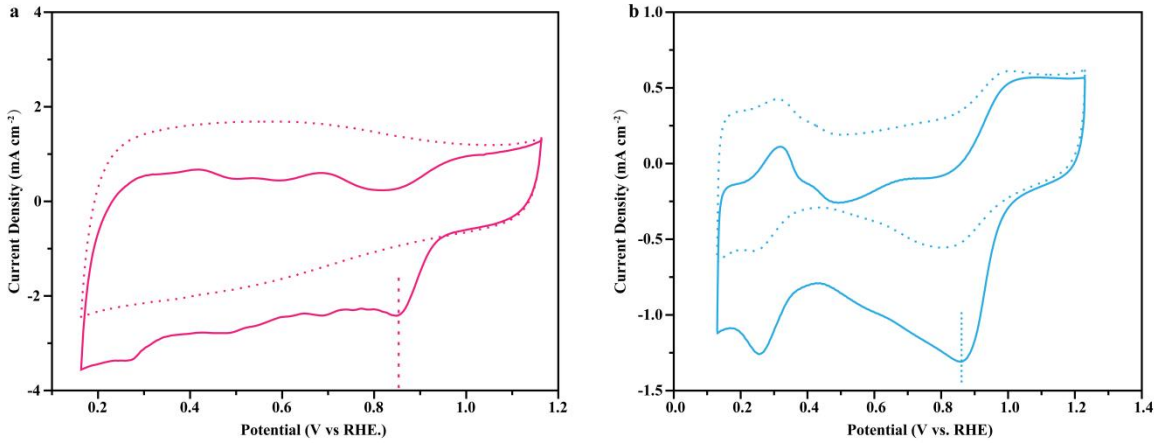

Supplementary Fig. 8 | a, The CV curves of Fe_{SAC}-NC in O_2 (solid) or Ar (dotted)-saturated 0.1M KOH. **b,** The CV curves of 20% Pt/C in O_2 (solid) or Ar(dotted)-saturated 0.1M KOH.

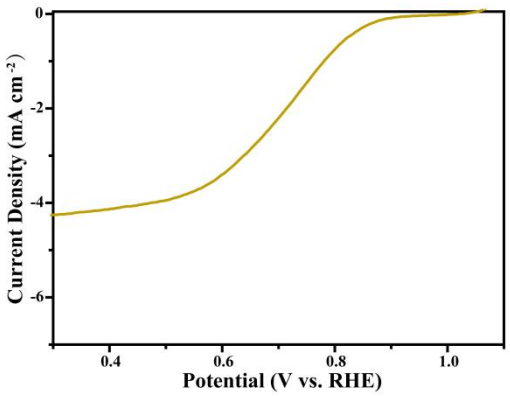

Supplementary Fig. 9 | LSV curve of NC.

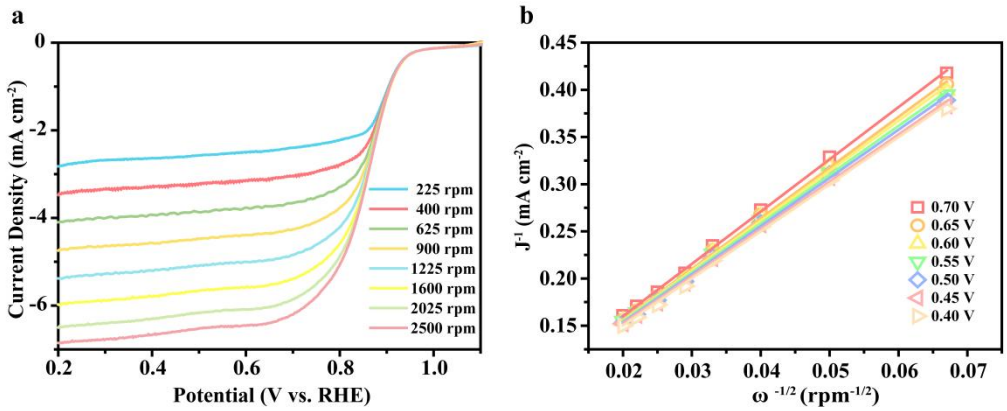

Supplementary Fig. 10 | a, LSVs curves of Fe_{SAC}-NC measured at different RDE rotating speed in O_2-saturated electrolytes. **b,** The corresponding K-L plot of Fe_{SAC}-NC.

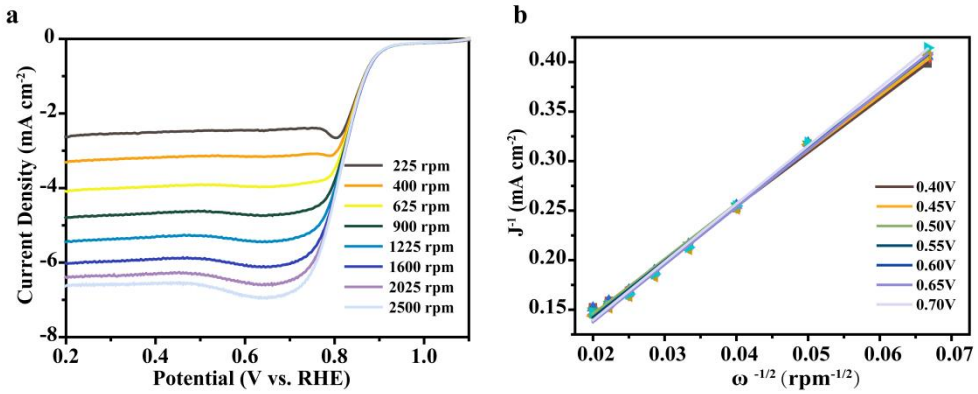

Supplementary Fig. 11 | a, LSVs curves of FeN_4 measured at different RDE rotating speed in O_2-saturated electrolytes. **b,** The corresponding K-L plot of FeN_4.

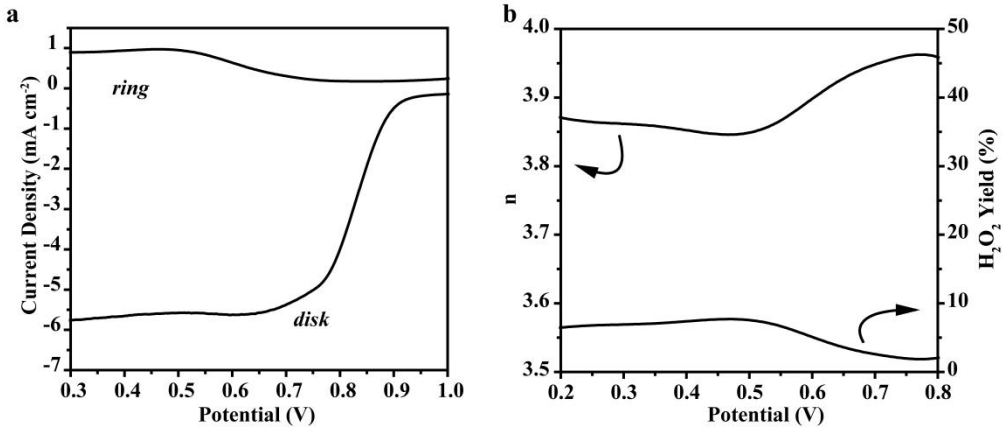

Supplementary Fig. 12 | a, RRDE test of FeN_4. **b,** Electron transfer number (n) and H_2O_2 yield calculated from RRDE measurement of FeN_4.

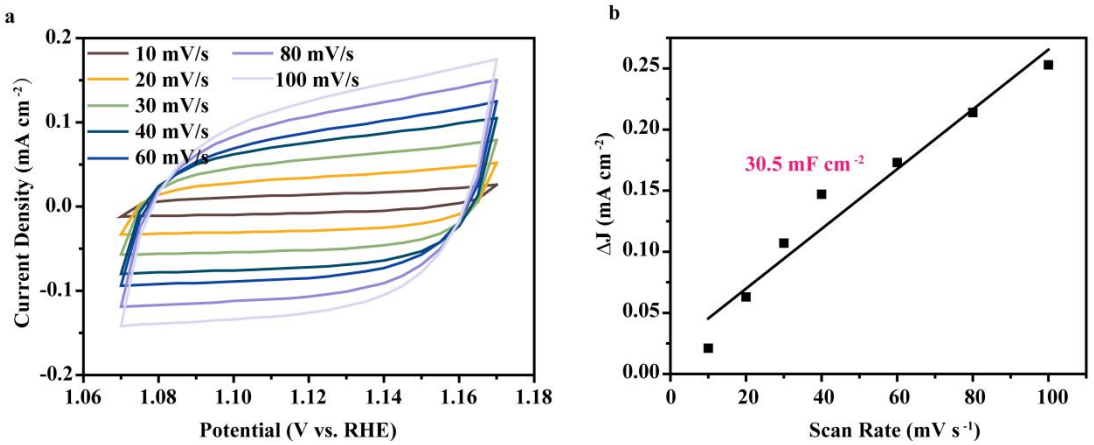

Supplementary Fig. 13 | a, CV curves for Fe_{SAC}-NC in the region of 1.06-1.18 V vs. RHE with various scan rates. **b,** Scan-rate dependency of the current density for Fe_{SAC}-NC.

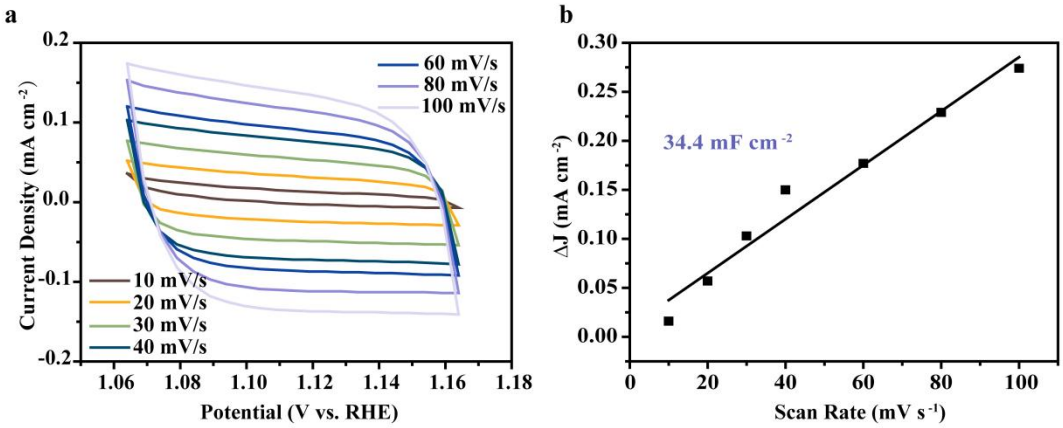

Supplementary Fig. 14 | a, CV curves for FeN_4 in the region of 1.06-1.18 V vs. RHE with various scan rates. **b,** Scan-rate dependency of the current density for FeN_4.

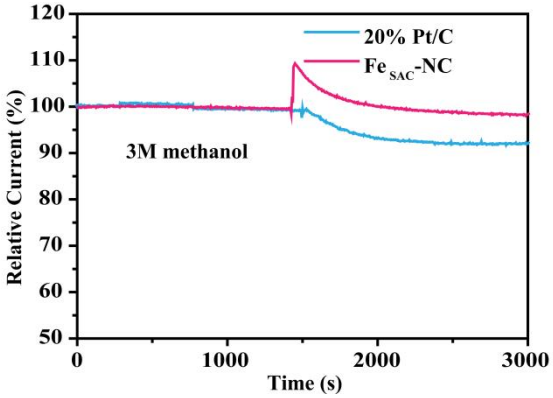

Supplementary Fig. 15 | Methanol crossover effect test of Fe_{SAC}-NC and 20% Pt/C.

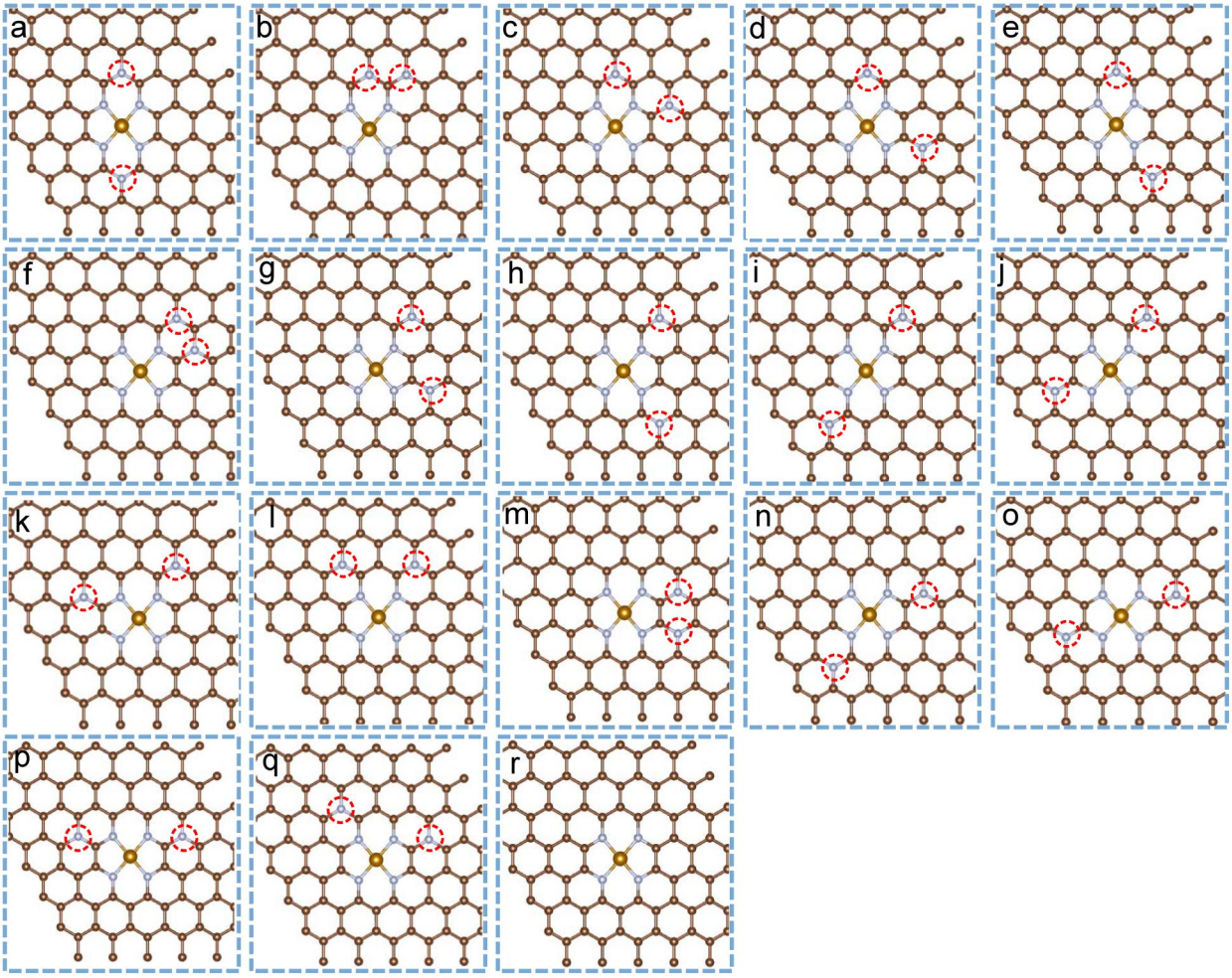

Supplementary Fig. 16 | Optimized structure of (**a**) Fe_{SAC}-N_1C. (**b**) Fe_{SAC}-N_2C. (**c**) Fe_{SAC}-N_3C. (**d**) Fe_{SAC}-N_4C. (**e**) Fe_{SAC}-N_5C. (**f**) Fe_{SAC}-N_6C. (**g**) Fe_{SAC}-N_7C. (**h**) Fe_{SAC}-N_8C. (**i**) Fe_{SAC}-N_9C. (**j**) Fe_{SAC}-$N_{10}C$. (**k**) Fe_{SAC}-$N_{11}C$. (**l**) Fe_{SAC}-$N_{12}C$. (**m**) Fe_{SAC}-$N_{13}C$. (**n**) Fe_{SAC}-$N_{14}C$. (**o**) Fe_{SAC}-$N_{15}C$. (**p**) Fe_{SAC}-$N_{16}C$. (**q**) Fe_{SAC}-$N_{17}C$. (**r**) FeN_4. (The names are derived from the N atoms respective locations.)

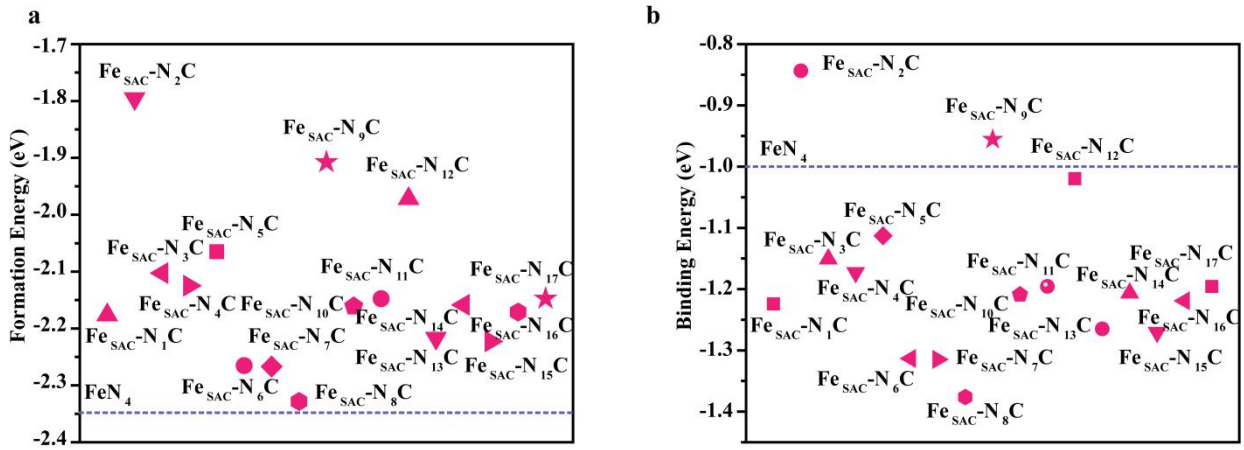

Supplementary Fig. 17 | a, The formation energy of Fe_{SAC}-N_XC (X=1-17). **b,** The binding energy of Fe site on Fe_{SAC}-N_XC (X=1-17).

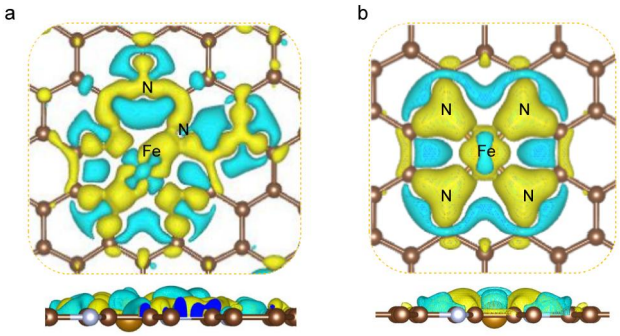

Supplementary Fig. 18 | a, Differential charge density of Fe_{SAC}-N_3C. **b,** Differential charge density of FeN_4. Yellow regions indicate charge accumulation, while cyan regions indicate charge depletion.

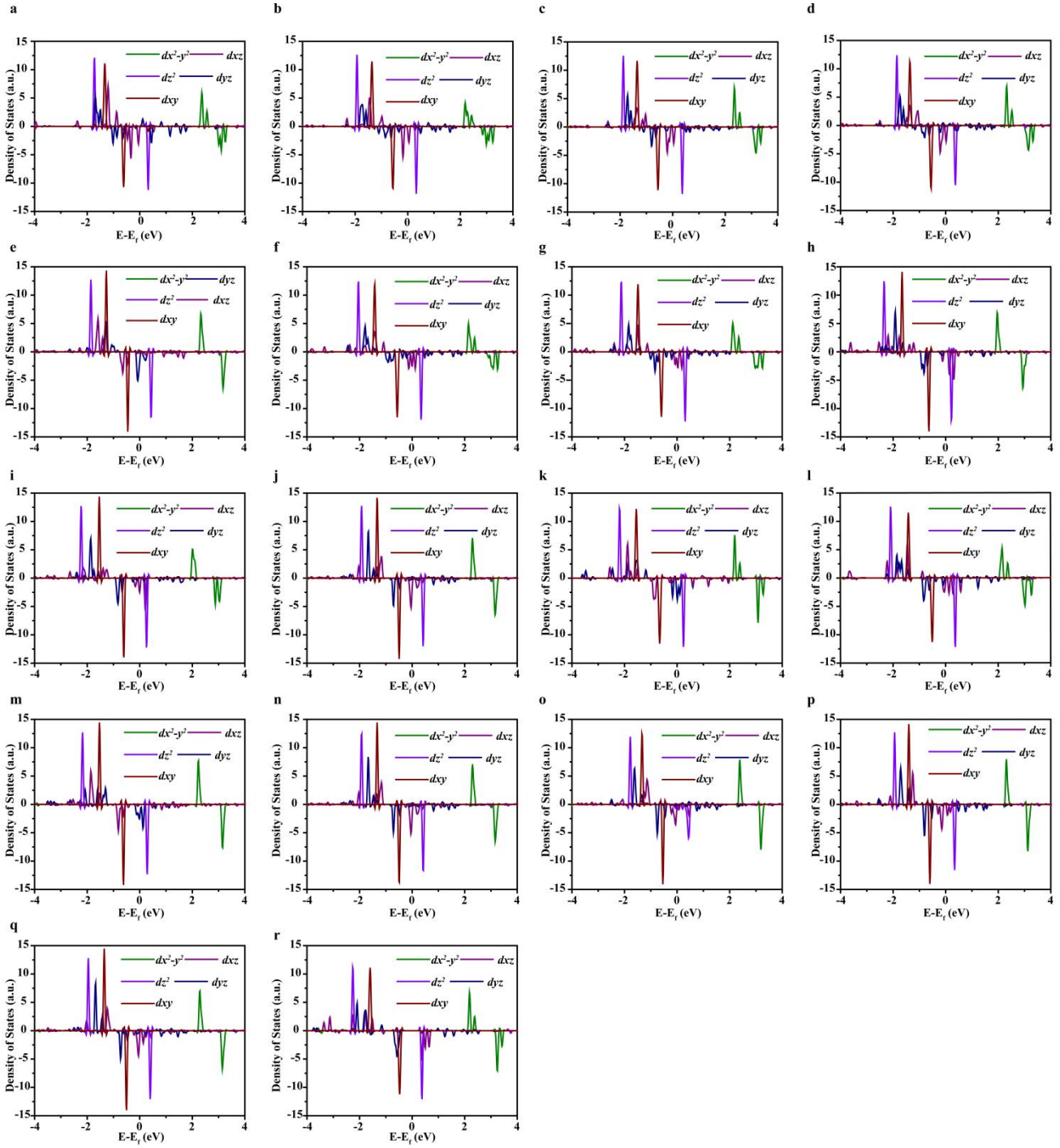

Supplementary Fig. 19 | Detailed DOS of Fe d orbitals: (**a**) Fe_{SAC}-N_1C, (**b**) Fe_{SAC}-N_2C, (**c**) Fe_{SAC}-N_3C, (**d**) Fe_{SAC}-N_4C, (**e**) Fe_{SAC}-N_5C, (**f**) Fe_{SAC}-N_6C, (**g**) Fe_{SAC}-N_7C, (**h**) Fe_{SAC}-N_8C, (**i**) Fe_{SAC}-N_9C, (**j**) Fe_{SAC}-$N_{10}C$, (**k**) Fe_{SAC}-$N_{11}C$, (**l**) Fe_{SAC}-$N_{12}C$, (**m**) Fe_{SAC}-$N_{13}C$, (**n**) Fe_{SAC}-$N_{14}C$, (**o**) Fe_{SAC}-$N_{15}C$, (**p**) Fe_{SAC}-$N_{16}C$, (**q**) Fe_{SAC}-$N_{17}C$ and (**r**) FeN_4.

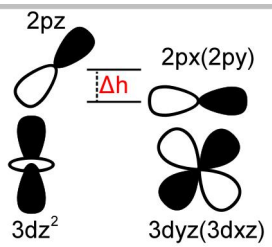

Supplementary Fig. 20 | Schematic illustration of different hybridization modes of *3dyz (3dxz), 3dz²* and OH 2π* orbital. (Δh means the spatial height difference.)

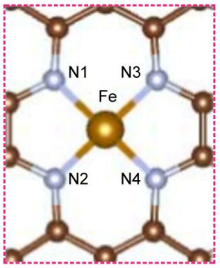

Supplementary Fig. 21 | The schematic of each Fe-N bond length of Fe_{SAC}-N_xC(x=1-17).

Supporting tables

Supplementary Table 1 | Summary of NC, Fe_{SAC}-NC, and FeN_4 BET data.

Sample	BET surface area ($m^2 \cdot g^{-1}$)	Total volume ($cm^3 \cdot g^{-1}$)	Mesopore size (nm)
NC	255	0.29	5.4
Fe_{SAC}-NC	725	1.66	15.4
FeN_4	752	3.77	21.2

Supplementary Table 2 | Elemental composition of Fe_{SAC}-NC.

elemental analyzer				ICP	TGA
C (wt.%)	N (wt.%)	O (wt.%)	H (wt.%)	Fe(wt.%)	
81.38	8.97	3.21	0.96	5.48	5.39

Supplementary Table 3 | EXAFS fitting parameters of Fe foil and Fe_{SAC}-NC.

Samples	Shell	N	R (Å)	$\Delta\sigma^2 \times 10^3$ ($Å^2$)	ΔE_0 (eV)	R-factor
Fe foil	Fe-Fe	8	2.42±0.01	6.8 ± 1.2	10.6 ± 0.8	0.037
	Fe-Fe	6	2.84±0.01	9.0 ± 2.1	10.1 ± 0.4	
FeN_4	Fe-N	4	1.89±0.01	3.1±1.6	1.2±0.1	0.019
Fe_{SAC}-NC	Fe-N	3.7	1.90±0.02	8.17± 1.1	-7.8±0.5	0.042

Supplementary Table 4 | Summarize the E_0 values of standard reference materials and Fe_{SAC}-NC.

Sample	Fe foil	Fe_2O_3	FeN_4	Fe_{SAC}-NC
E_0 (eV)	7112.216	7126.305	7122.311	7123.292

Supplementary Table 5 | Summarize the most near-term reported single atoms-based electrocatalysts.

Sample	Onset potential (V vs. RHE)	Half-wave potential (V vs. RHE)	Ref
Fe_{SAC}-NC	1.06	0.89	our work
Ru-SAS/SNC	0.998	0.861	**1**
Cu/Zn-NC	0.98	0.83	**2**
Co-N/C+NG	1.04	0.915	**3**
Fe-N-CDC/CNT	0.99	0.86	**4**
Fe-NiNC-50	1.0	0.84	**5**
FeSA/HNPC	0.92	0.83	**6**
Cu-S_1N_3	1.05	0.918	**7**
Ni-N_4/GHSs/Fe-N_4	0.93	0.83	**8**
Co_1-N_3PS/HC	1.00	0.91	**9**
PSTA-Co-1000	0.96	0.878	**10**
Fe-N/P-C-700	0.941	0.867	**11**
Fe/OES	1.00	0.85	**12**

Supplementary Table 6 | Adsorption free energies of *O, *OH, and *OOH on Fe_{SAC}-N_XC(X=1-17).

Catalysts	ΔG_{*O} (eV)	ΔG_{*OH} (eV)	ΔG_{*OOH} (eV)
Fe_{SAC}-N_1C	1.93	0.84	3.56
Fe_{SAC}-N_2C	1.74	0.86	3.54
Fe_{SAC}-N_3C	1.70	0.84	3.60
Fe_{SAC}-N_4C	1.81	0.86	3.51
Fe_{SAC}-N_5C	1.70	0.80	3.52
Fe_{SAC}-N_6C	1.66	0.86	3.48
Fe_{SAC}-N_7C	1.65	0.83	3.48
Fe_{SAC}-N_8C	1.65	0.85	3.49
Fe_{SAC}-N_9C	1.66	0.84	3.53
Fe_{SAC}-$N_{10}C$	1.66	0.82	3.53
Fe_{SAC}-$N_{11}C$	1.66	0.86	3.61
Fe_{SAC}-$N_{12}C$	1.75	0.82	3.49
Fe_{SAC}-$N_{13}C$	1.65	0.75	3.40
Fe_{SAC}-$N_{14}C$	1.65	0.83	3.49
Fe_{SAC}-$N_{15}C$	1.77	0.82	3.51
Fe_{SAC}-$N_{16}C$	1.76	0.85	3.53
Fe_{SAC}-$N_{17}C$	1.66	0.84	3.50
FeN_4	1.39	0.58	3.56

Supplementary Table 7 | Reaction free energy of elementary step for ORR at U = 0 V vs. RHE on Fe_{SAC}-N_XC(X=1-17).

Catalysts	ΔG_1 (eV)	ΔG_2 (eV)	ΔG_3 (eV)	ΔG_4 (eV)	ΔG_5 (eV)
Fe_{SAC}-N_1C	-0.51	-0.85	-1.63	-1.09	-0.84
Fe_{SAC}-N_2C	-0.52	-0.86	-1.80	-0.87	-0.86
Fe_{SAC}-N_3C	-0.55	-0.76	-1.90	-0.86	-0.84
Fe_{SAC}-N_4C	-0.55	-0.86	-1.82	-0.90	-0.80
Fe_{SAC}-N_5C	-0.52	-0.89	-1.70	-0.95	-0.86
Fe_{SAC}-N_6C	-0.70	-0.74	-1.82	-0.80	-0.86
Fe_{SAC}-N_7C	-0.50	-0.94	-1.83	-0.82	-0.83
Fe_{SAC}-N_8C	-0.42	-1.01	-1.84	-0.80	-0.85
Fe_{SAC}-N_9C	-0.46	-0.93	-1.87	-0.82	-0.84
Fe_{SAC}-$N_{10}C$	-0.51	-0.87	-1.88	-0.83	-0.82
Fe_{SAC}-$N_{11}C$	-0.71	-0.72	-1.85	-0.89	-0.86
Fe_{SAC}-$N_{12}C$	-0.67	-0.84	-1.82	-0.84	-0.82
Fe_{SAC}-$N_{13}C$	-0.54	-0.98	-1.75	-0.90	-0.75
Fe_{SAC}-$N_{14}C$	-0.53	-0.90	-1.84	-0.82	-0.83
Fe_{SAC}-$N_{15}C$	-0.53	-0.88	-1.74	-0.95	-0.82
Fe_{SAC}-$N_{16}C$	-0.53	-0.87	-1.77	-0.91	-0.85
Fe_{SAC}-$N_{17}C$	-0.53	-0.89	-1.84	-0.82	-0.84
FeN_4	-0.70	-0.67	-2.17	-0.81	-0.58

Supplementary Table 8 | Fe-N1, Fe-N2, Fe-N3, Fe-N4 and the average Fe-N bond length over Fe-N-C catalysts.

Catalysts	Fe-N1 (Å)	Fe-N2 (Å)	Fe-N3 (Å)	Fe-N4 (Å)	Average Fe-N (Å)
Fe_{SAC}-N_1C	1.90	1.90	1.90	1.90	1.90
Fe_{SAC}-N_3C	1.91	1.90	1.91	1.89	1.90
Fe_{SAC}-N_4C	1.90	1.90	1.89	1.91	1.90
Fe_{SAC}-$N_{16}C$	1.92	1.89	1.92	1.89	1.91

Supplementary References

1. Qin, J. *et al.* Altering ligand fields in single-atom sites through second-shell anion modulation boosts the oxygen reduction reaction. *J. Am. Chem. Soc.* **144**, 2197-2207, (2022).
2. Tong, M. *et al.* Operando cooperated catalytic mechanism of atomically dispersed Cu-N_4 and Zn-N_4 for promoting oxygen reduction reaction. *Angew. Chem. Int. Ed.* **60**, 14005-14012, (2021).
3. Zhang, X. *et al.* Boosting electrocatalytic activity of single atom catalysts supported on nitrogen-doped carbon through N coordination environment engineering. *Small* **18**, e2105329, (2022).
4. Lilloja, J. *et al.* Transition-metal- and nitrogen-doped carbide-derived carbon/carbon nanotube composites as cathode catalysts for anion-exchange membrane fuel cells. *ACS Catal.* **11**, 1920-1931, (2021).
5. Zhu, X. *et al.* Harnessing the interplay of Fe-Ni atom pairs embedded in nitrogen-doped carbon for bifunctional oxygen electrocatalysis. *Nano Energy* **71**, 104597-104607, (2020).
6. Jin, X. *et al.* A highly efficient Fe-N-C electrocatalyst with atomically dispersed FeN_4 sites for the oxygen reduction reaction. *ChemCatChem* **13**, 2683-2690, (2021).
7. Shang, H. *et al.* Engineering unsymmetrically coordinated Cu-S_1N_3 single atom sites with enhanced oxygen reduction activity. *Nat. Commun.* **11**, 3049, (2020).
8. Chen, J. *et al.* Dual single-atomic Ni-N_4 and Fe-N_4 sites constructing janus hollow graphene for selective oxygen electrocatalysis. *Adv. Mater.* **32**, e2003134, (2020).
9. Chen, Y. *et al.* Atomic-level modulation of electronic density at cobalt single-atom sites derived from metal-organic frameworks: enhanced oxygen reduction performance. *Angew. Chem. Int. Ed.* **60**, 3212-3221, (2021).
10. Wei, X. *et al.* Cross-linked polyphosphazene hollow nanosphere-derived N/P-doped porous carbon with single nonprecious metal atoms for the oxygen reduction reaction. *Angew. Chem. Int. Ed.* **59**, 14639-14646, (2020).
11. Yuan, K. *et al.* Boosting oxygen reduction of single iron active sites via geometric and electronic engineering: nitrogen and phosphorus dual coordination. *J. Am. Chem. Soc.* **142**, 2404-2412, (2020).
12. Hou, C.-C. *et al.* Single-atom iron catalysts on overhang-eave carbon cages for high-performance oxygen reduction reaction. *Angew. Chem. Int. Ed.* **59**, 7384-7389, (2020).